DESIGN AND AERODYNAMIC PERFORMANCE OF A HIGH PRESSURE AXIAL FLOW FAN

Vaclav CYRUS, Jan CYRUS, Pavel PANEK

AHT Energetika Ltd, Podnikatelska 550, 190 11 Praha 9- Bechovice,

Czech Republic

SUMMARY

The investigated fan stage with a hub/tip ratio of 0.6 has design flow and pressure coefficients of 0.6 and 0.83, respectively. Test and computed aerodynamic performance of the axial flow fan and the fan stage is compared. The fan consists of an axial flow stage, an inlet chamber and a diffuser. Two variations of chamber struts were tested. Reduced number of struts and their thickness lower the chamber loss coefficient thus the fan efficiency increases. Near the fan stability limit the diffuser loss coefficient increases because of the inlet velocity profile distortion.

INTRODUCTION

Modern coal fired power stations fitted with desulphurization equipment require axial flow fans with high flow rates and high pressure ratio. More often than not, each boiler block has one or two air fans and one to three flue gas fans. Currently, most of the boiler blocks are gradually being refurbished. New blocks with an electrical power output of 500 to 700 MWe are at proposal and design stages thus the high pressure fan stage blading has to be designed using the latest design techniques applied to the axial compressors, e.g. Broedersen [1], Baumgarten et al. [2] and Cyrus et al. [3], [4], [5].

Our paper deals with an aerodynamic performance of a complete one stage axial flow fan consisting of an axial flow stage, an inlet suction chamber and an exhaust diffuser. The axial flow stage with the hub/tip ratio of 0.6 is highly aerodynamically loaded. The analysis of the aerodynamic performance the of stage blading, the inlet chamber and the diffuser with the use of the flow simulation and test results is carried out. This problem is not solved in open literature. The inlet chamber struts design, based on the CFD results, is also discussed in our paper.

AXIAL FLOW FAN DESIGN

Axial flow fan stage

The axial fan stage geometry was derived using the CADAC design code for the axial flow compressor stage. Axisymmetric flow solution is based on the streamline curvature method; the

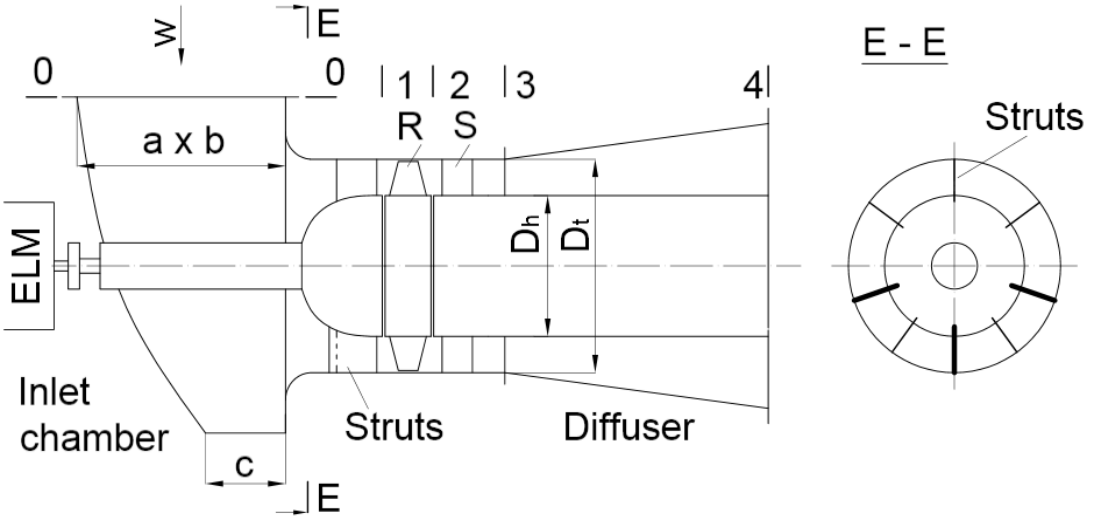

Figure 1: Axial flow fan diagram

aerodynamic performance of the blade element is derived using the Lieblein method [6] with secondary losses calculated for the blade with and without the tip clearance, Cyrus [3]. Flow in the inlet and outlet planes is axial. CFD method (NUMECA commercial program [7]) was used in the aerodynamic performance calculations of a new stage.

The outer and inner diameters of our stage were constant with the external diameter being 600 mm. The hub/tip ratio of the stage blading was $\nu = 0.60$. The stage consisted of the rotor and stator rows (Fig.1) and had the design flow coefficient $\varphi_D = 0.60$ and the design pressure coefficient $\psi_D = 0.83$. Profiles of the rotor and stator airfoils were NACA 65 series with the reinforced trailing edge and the circular camber lines. The rotor and stator rows have 22 and 31 blades, respectively. In order to obtain acceptable aerodynamic loading of the rotor blade elements near the hub, the smaller fan work redistribution along the radius was applied. The relative difference of the total enthalpy increase at the hub was lower than at casing, $(\Delta H_t - \Delta H_h) / \Delta H_m = 6$ %, for the new stage.

Graphs of the diffusion factor DF of the rotor and stator blade elements, shown in Fig. 2, were attained by use of the design code. The diffusion factor values DF of both blade rows are below the critical value DF = 0.60 valid for the plane cascades. The maximum values of the rotor and stator rows diffusion factor were DF = 0.55 and 0.57, respectively. In order to retain these DF values on the hub of the stator blade elements, it was required to apply relatively high cascade solidity $\sigma = c/s = 2.9$. The blade aspect ratio AR = h/c of the rotor and stator blade rows was AR = 1.17 and 1.26, respectively.

The relative height of the radial clearance between the rotor blade tip and the casing was not constant along the stage axis. Near the rotor blade axis the ratio of the tip clearance s_r and the chord length was $c - s_r/c = 0.008$. At the leading and trailing edges, the radial clearance was higher - $s_r/c = 0.018$ to enable the rotor blade resetting.

Inlet chamber and diffuser

An exhaust diffuser had the area ratio of $A_4/A_3 = 1.87$ and the inlet chamber with parameters of $b/a = 1.28$ and $a/D_t = 1.25$. Rectangular side a is parallel with the fan axis (Fig.1). The shape of the standard chamber was aerodynamically optimized. The casing hub was supported by struts. Two versions of strut length and thickness were considered in our investigations. The standard version had 5 short and thin (dashed line) and 3 long and thick struts (full line), see Fig.1.

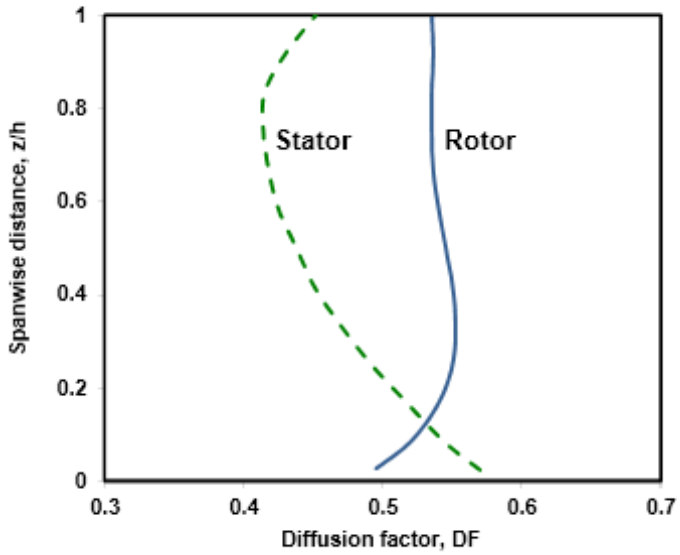

Figure 2: Diffusion factor spanwise distributions

The ratio of strut thicknesses is d_{long}/d_{short} = 5. The application of longer struts increases bearing support stiffness. The second version has only 6 short (dashed line) and thin struts and it is considered as ideal from the aerodynamic point of view.

Effect of the inlet chamber and diffuser losses on the axial flow fan aerodynamic performance

In the Appendix the relationship of the aerodynamic performance of the fan stage blading (R+S) and the complete axial flow fan is derived, it is based on one-dimensional flow model. Equations (2) and (3) show that the fan efficiency η_F and the pressure coefficient ψ_F decrease with the energy losses of the inlet chamber and the diffuser ($\zeta_{IC} + \zeta_D$) and the flow coefficient φ. This tendency is weakened by the increase of the fan stage blading pressure coefficient ψ_{ST}. It follows from Appendix that fan operating points should be located within performance characteristics field that has low value of the flow coefficient in order to attain high fan efficiency. Low energy losses requirement in the fan inlet and outlet, is of crucial importance.

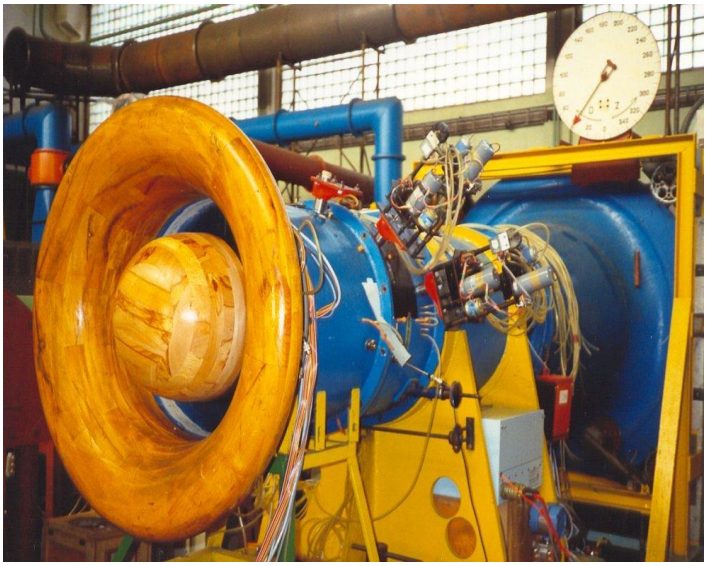

Figure 3: Test rig

EXPERIMENTAL INVESTIGATIONS OF FAN AND FAN STAGE BLADING

Our investigation was carried out in two phases. During the first phase the blading performance was measured on a test rig, see Fig. 3, with an external diameter of 600 mm. The inlet nozzle to measure the flow rate was located at the equipment front. The radial diffuser, located at the outlet, had moveable rear wall which made it possible to alter the aerodynamic resistance. The rig was driven by a DC motor with a swinging stator to measure torque by weighing.

The aerodynamic performance of the complete fan consisting of the stage blading with the external diameter of 600 mm, the inlet suction chamber and the exhaust diffuser was measured on the test rig built in compliance with the ISO standards [12]. The complete fan was connected to a piping system equipped with throttle control equipment. The flow rate was determined with the aid of a standard orifice. To find the reliable fan efficiency measurement of the dynamometer torque was taken.

Both tests were carried out at 1800 1/min; this relates to the inlet Mach number of stage blade rows $Ma_1 < 0.30$ and the Reynolds number $Re_u = u_t\, c/\, \nu = 400x10^3$. The fan working points were calculated with the use of the average values of the flow properties in the inlet and outlet planes of the stage blading and axial flow fan. The stability limit of tested stages was found by the use of the unsteady pressure transducers placed in the plane behind the rotor blade row on the casing. Rotating stall appeared in the unstable part of the stage operational performance.

Uncertainty of the calculation of the fan efficiency κ_η was derived using the uncertainty analysis: $\pm \kappa_\eta = \pm$ 1.0 to 1.5%. Higher and lower κ_η is associated with the working conditions of $\varphi = 0.453$ to 0.5 and 0.6 to 0.8, respectively. Measurement errors of the following properties were considered in the uncertainty analysis: pressure ±5 Pa, temperature ±0.3K, flow angle $\pm 1^o$, torque ± 0.08 Nm.

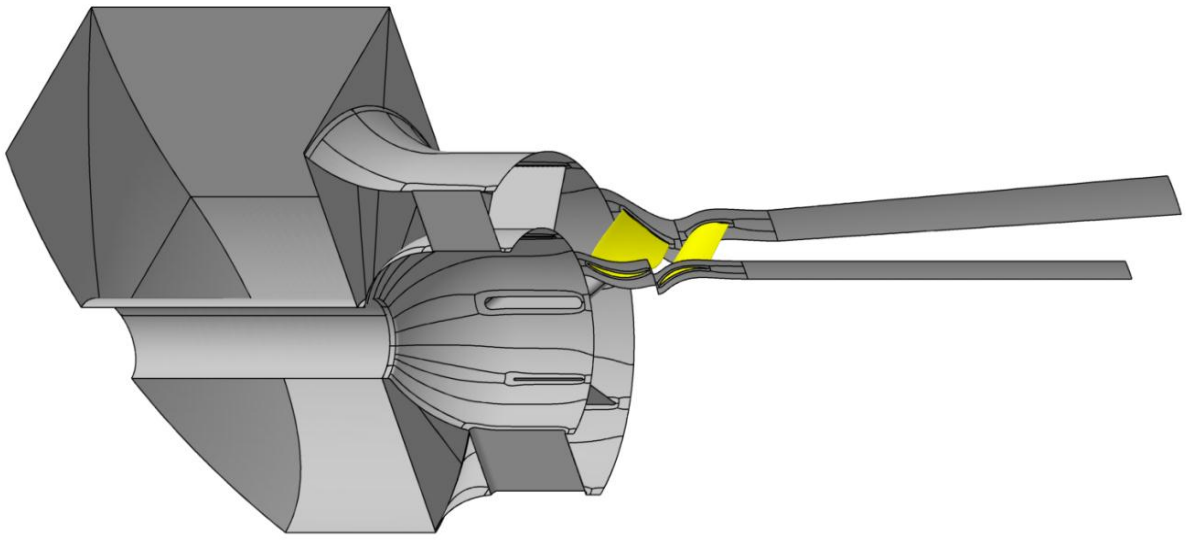

Figure 4: Computational model of complete axial flow fan

FLOW SIMULATIONS IN AXIAL FLOW FAN

The NUMECA code [7] solves Reynolds-averaged Navier-Stokes equations of the structured multi block grid topologies with the mixing planes between adjacent blade rows. An explicit time marching 4 step Runge Kutta procedure with the implicit residual smoothing was employed. A cell centered second order finite volume discretization was used. The local time stepping and multi grid capability were available to enhance convergence. The Spalart-Allmaras turbulence model was used.The code is frequently used in the performance prediction of industrial fans and turbocompressors, e.g. [8], [9].

The computational grids consisted of 2.4 to 2.8 million cells, which were distributed among the five principal parts of the domain: the inlet region, the strut section, the rotating and stationary blades, and the outlet diffuser (Fig.4). The inlet region was comprised of three blocks totaling 650, 000 cells and started at the air intake into the domain in the direction perpendicular to the machine axis. The section with radial struts was connected to the inlet region by the means of a full non matching interface, which is used to resolve the boundary between two regions with different interface geometry. The strut section was modular and was replaced in each calculated version; each strut passage consisted of five blocks and 350, 000 cells. In order to take advantage of the domain lateral symmetry, only a 180 degree section of the inlet region and struts was modeled; to enable this, the strut passage blocks were cut in half at the symmetry plane. The rotating and stationary blade rows were attached to the strut section and to each other via the mixing plane interface, therefore only one blade of the rotating and stationary rows each was modeled. The rotating blade passage consisted of seven blocks totaling 330, 000 cells, including a radial gap with two blocks and 30, 000 cells. The stationary blade passage consisted of five blocks and 260, 000 cells, while the single outlet diffuser block contributed with additional 145, 000 cells. The cell width, at walls, was kept in the 0.03 to 0.07 mm range in all cases to ascertain that the wall y+ does not exceed 5.

A mass flow boundary condition was imposed at the inlet; its value was changed depending on the point on the performance graph that was being calculated. At the exit from the diffuser block a fixed static pressure condition was set. A no-slip boundary condition was imposed at walls, along with the wall rotation speed where applicable. The air was modeled as perfect gas.

The convergence was calculated using the computation of residuals. In the end, the residuals are of the order 10^{-6}. The convergence of the fan efficiency was also considered.

DISCUSSION OF ACQUIRED RESULTS

Aerodynamic performance of the stage blading and the complete fan

Fig. 5 shows comparison of the test graphs of the pressure coefficient ψ and the relative efficiency η / η_{ref} of the stage blading and the axial fan on the flow coefficient φ. The efficiency η_{ref} reference value is the maximum test value of the stage blading efficiency. The fan inlet chamber struts were of the standard design. It is evident that the difference between the aerodynamic performance of the stage and the complete fan increases with the increase of the flow coefficient φ, as it follows from equations (2) and (3) shown in the Appendix. When the design value of the flow coefficient is φ_D = 0.60, the difference of the relative values of the efficiency is $(\eta_{ST} - \eta_F)/\eta_{ref}$ = 7.2%. At the design point we measured the stage pressure coefficient ψ as 0.86 which is slightly higher that the design value ψ_D = 0.83.

Fig. 5 also shows graphs derived from the results of the flow simulation. We calculated the aerodynamic performance for 5 values of the flow coefficient. The agreement between the calculated and test graphs for the axial fan is considered as acceptable.

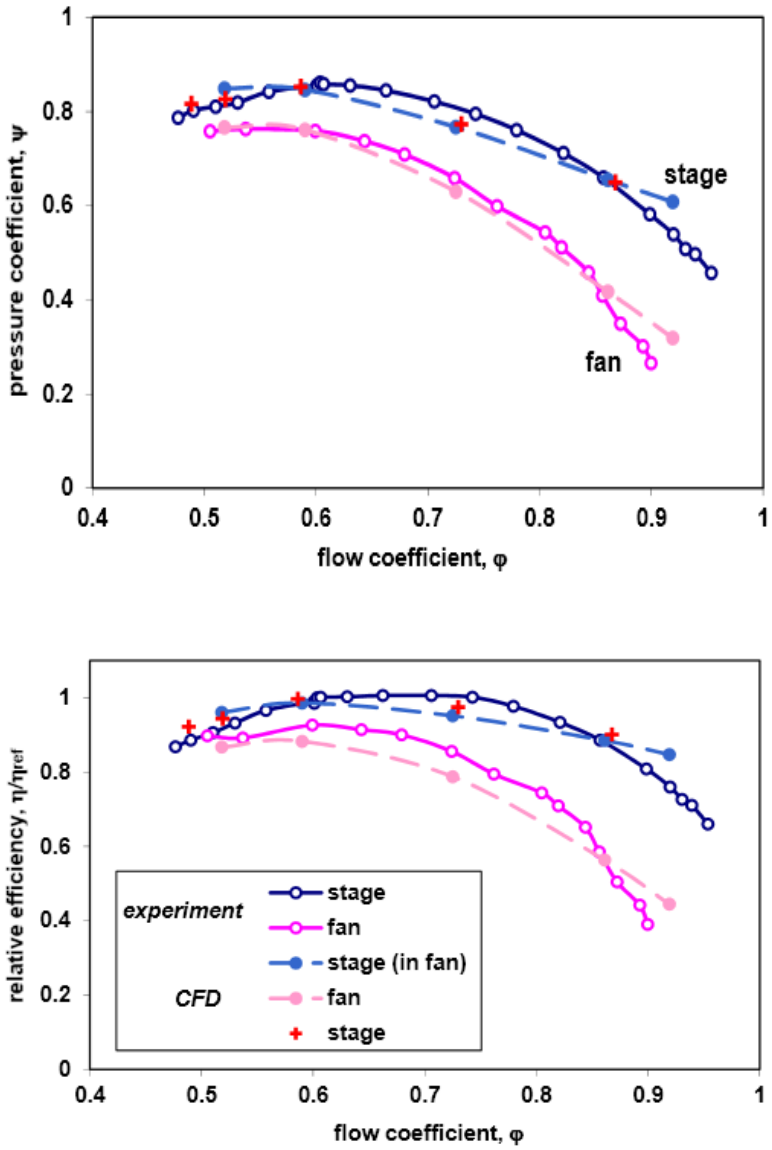

Figure 5: Fan and fan stage aerodynamic performance

Table 1: Aerodynamic performance of axial fan

	η_F / η_{ref}		ψ_F	
φ	0,60	0,86	0,60	0,86
Var. No.1	0,881	0,563	0,761	0,417
Var. No.2	0,889	0,588	0,767	0,432

In the Table No. 1 we compared the relative efficiency η_F / η_{ref} and the pressure coefficient ψ_F of a fan with two inlet chambers with the use of the flow simulation data. It is clear that if we use an ideal chamber with 6 thin struts the relative efficiency η_F / η_{ref} increases, with the flow coefficient being $\varphi = 0.60$, by 0.8 %. For a higher value of the flow coefficient $\varphi = 0.86$ the increase is 2.5%.

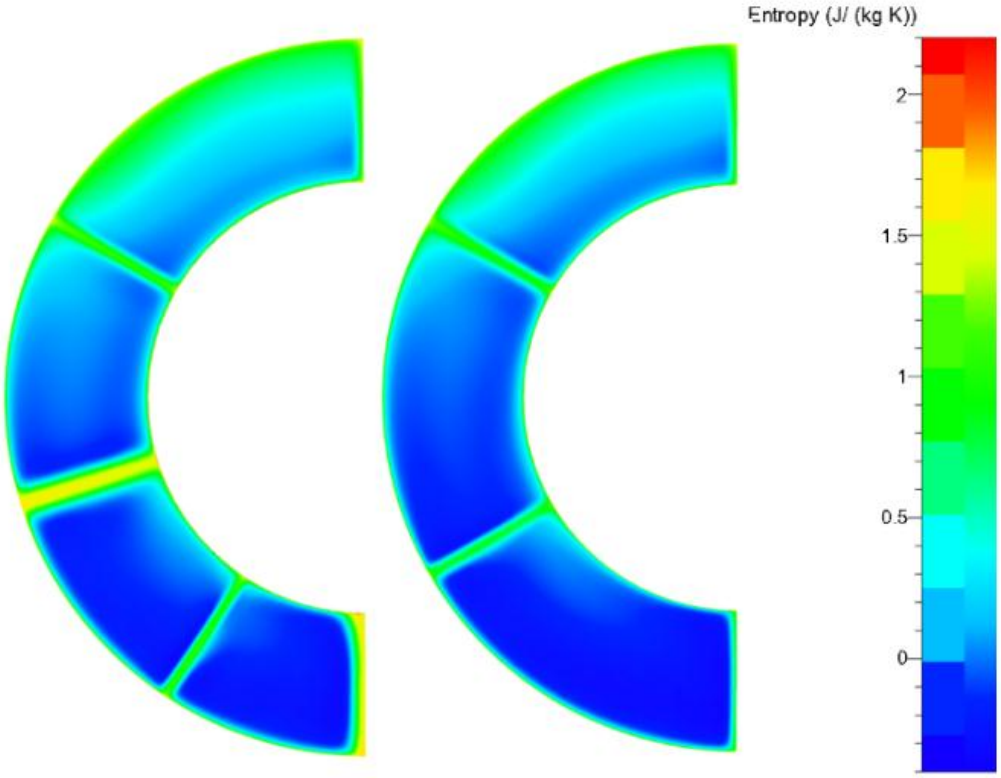

(a) Standard variant (b) Ideal variant

Figure 6: Entropy distribution in plane behind inlet casing

Similarly, the increase of the pressure coefficient ψ_F increases with the growth of the flow coefficient.

Fig. 5 shows computed points valid for the isolated stage (marked by crosses) as well as for the fan inbuilt stage (marked by full circles). We are reminded that the test points were measured on the isolated stage of the test rig, as shown in Fig. 3. The difference between the computed variables is relatively small and is similar to the measurement uncertainties. Higher values of the efficiency and the pressure coefficients were derived for the isolated stage, because the inlet velocity profile is smooth and flow is axially symmetrical in comparison with the fan stage. We can observe small difference between experimental and computed stability limits of both configurations. It can be also explained by different inlet flow conditions of rotor blade row in the case of isolated stage and complete fan [2] .

Aerodynamic performance of the inlet chamber and the diffuser

The Table No. 2 shows the loss coefficient of the inlet suction chamber ζ_{IC} and the diffuser ζ_D relating to the three typical values of the flow coefficient $\varphi = 0.52$, 0.60 and 0.86 and two versions of the inlet chamber, standard (8 struts) and ideal (6 struts). The loss coefficient values were derived from the average values of the total pressure in Planes 0, 1, 3 and 4 (Fig. 1).

For a given version of the inlet chamber the coefficient ζ_{IC} slightly decreases with the gas flow increase. This apparently relates to the influence of the Re number. For the standard version the loss coefficient is approximately 0.035 higher than for the ideal one; it is associated with the flow around the struts as it is shown in Fig. 6a and 6b. Higher entropy is noticeable behind the longer and

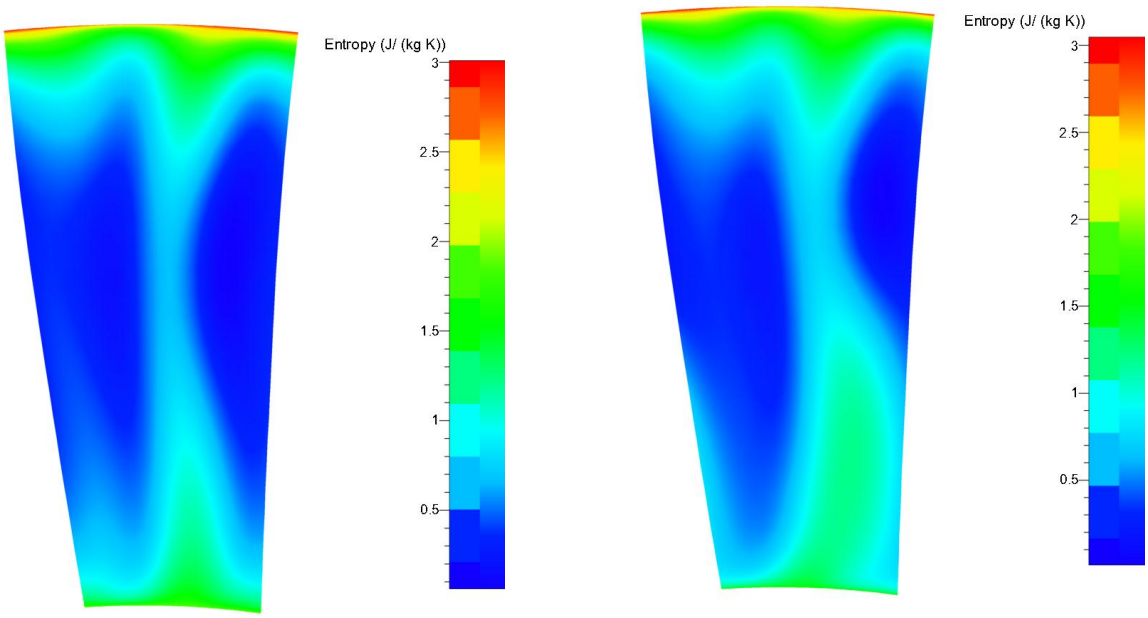

(a) φ = 0,60 (b) φ = 0,52

Figure 7: Entropy distribution in plane behind stator blade row

Table 2: loss coefficients of inlet chamber and diffuser

	ζ_{IC}			ζ_D		
φ	0,52	0,60	0,86	0,52	0,60	0,86
Var. No.1	0,135	0,133	0,124	0,071	0,050	0,051
Var. No.2	0,099	0,098	0,092	0,070	0,052	0,051

thicker struts as it can be seen in Fig. 6a. Both versions have noticeable higher entropy in the upper part of the chamber as a result of more acute flow path change.

The diffuser loss coefficients shown in the Table No. 2 are practically same $\zeta_D = 0.050 – 0.052$ with the flow coefficient φ = 0.60 and 0.86, for the fans with two versions of the inlet chamber. However, at the operating point prior to the stability limit, the coefficient increases by approximately $\Delta\zeta_D = 0.02$. This relates to the flow conditions in the inlet diffuser plane.

Fig. 7 and Fig. 8 show the entropy contours in the plane located behind the stator row and the diffuser with the flow coefficient φ = 0.60 and 0.52. When comparing Fig. 7a and Fig. 7b it is evident that the entropy generation in the stator row is higher in the lower part of blade near the stability limit (φ = 0.52) than at the design condition (φ = 0.60). It relates to the larger flow separation on the suction blade surface due to higher incidence angles. This deforms the diffuser inlet velocity profile, as it is evident from Fig. 9. The flow inlet angle α is slightly changed as it can be seen in Fig. 10.

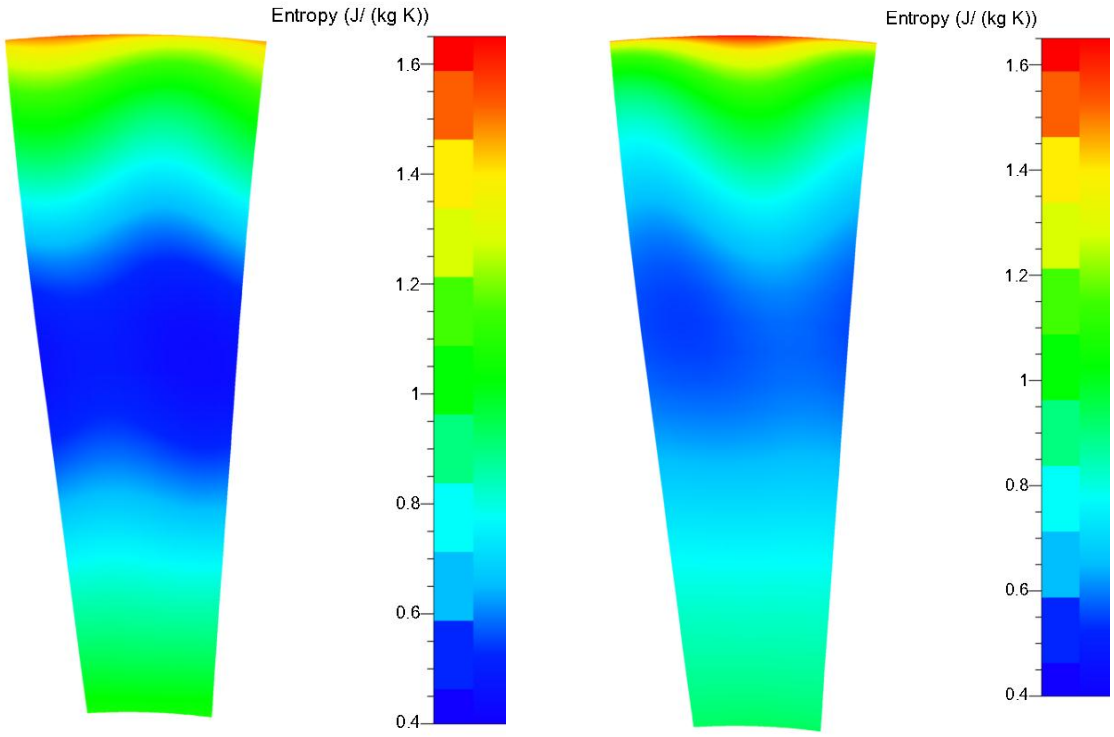

(a) φ = 0,60 (b) φ = 0,52

Figure 8: Entropy distribution in plane behind diffuser

From the comparison of the entropy distribution in the diffuser outlet plane shown in Fig. 8a and Fig. 8b it follows that the entropy generation increase in the diffuser occurs practically in the whole cross-section of the flow channel when there is an increased deformation of the inlet velocity profile, with φ = 0.52. The results are in agreement with the previous published works relating to the turbomachines diffusor aerodynamics, e.g. [10], and [11].

CONCLUSIONS

We designed the high pressure axial fan stage with high aerodynamic loading. The hub/tip ratio was 0.6. Design value of the pressure coefficient and the flow coefficient was 0.83 and 0.60, respectively. Our paper shows the test and calculated aerodynamic performance graphs of the fan stage as well as of the complete fan which comprises from the fan stage, the inlet chamber and the diffuser. Calculations were based on the flow numerical simulation (CFD Numeca). From the results we derived the energy losses in the inlet chamber and diffuser. The key conclusions are summarised below:

i) Test results proved compliance with the design assumptions of the fan stage

ii) We reached an acceptable agreement between calculated and test runs of the aerodynamic performance of the fan stage and the complete fan

iii) Efficiency difference between the fan stage and the complete fan increases with the flow coefficient. This is confirmed by derived relationships

iv) The inlet chamber loss coefficient is practically unchanged with the change of the flow coefficient. Reduction in the number of struts and their thickness led to the decrease of the inlet chamber loss coefficient of approximately 0.04 in relation to the standard version of the strut arrangement. This was reflected in the increase of the fan relative efficiency of 0.8% and 2.5% at design flow coefficient of $\varphi = 0.6$ and off-design flow coefficient $\varphi = 0.86$, respectively.

v) The diffuser loss coefficient increases with the flow decrease between the design point and the stability limit. This evidently relates to the flow field deformation at the diffuser inlet as a result of the more extensive flow separation origin in the stator row.

vi) It is recommended that further flow analysis of the complete fan is carried out with the use of the flow simulation especially for the outside the design systems operations when the rotor blades stagger is changed.

ACKNOWLEDGEMENT

The authors wish to acknowledge the support and grants from the Czech Ministry of Industry and Trade (MPO) – No.2A-1TP1/052, FR-TI1/347 and the Czech Grant Agency - No.101/ 09 /1959 and IAA200760801. The experiments were carried out on the ZVVZ company test rigs. Authors are grateful for it.

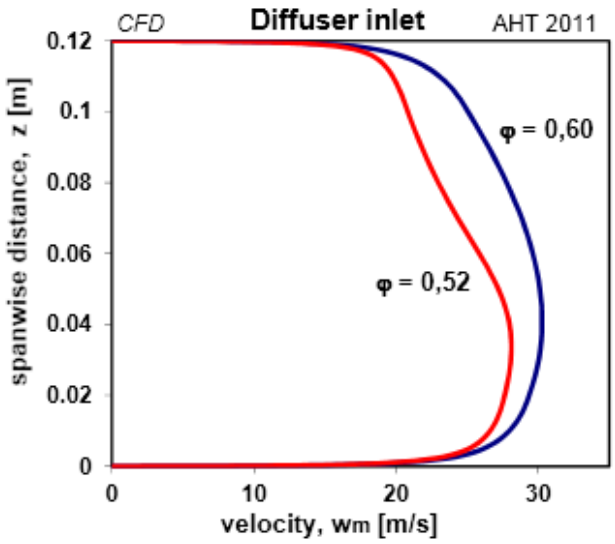

Figure 9: Velocity profiles in inlet plane of diffuser

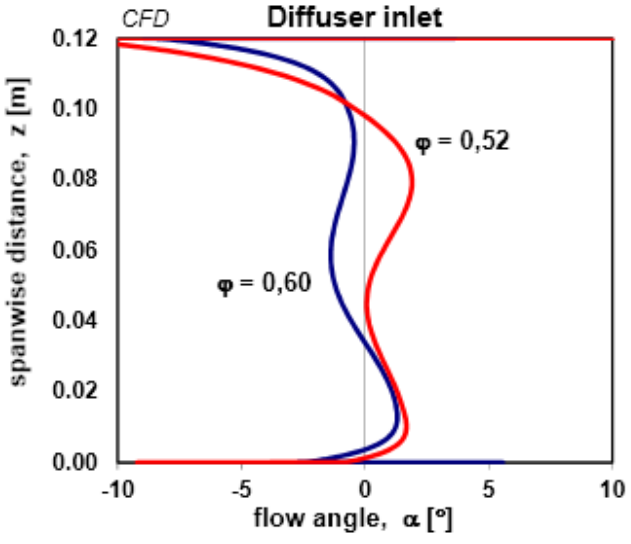

Figure 10: Flow angle in inlet plane of diffuser

BIBLIOGRAPHY

[1] S. Broedersen – *Experimental investigations on extremely loaded axial flow stages.* ASME Paper No.86-GT-116, ASME conference Turbo Expo,Dusseldorf, **1986**

[2] S. Baumgarten, H. Krasmann, J.Roesener - *Stand der Forschung an aerodynamisch Hochbelasteten Axialventilatoren am Pfleiderer Institute*, Mitteilungen TU Braunschweig, No.1, pp.147-160, **1994**

[3] V.Cyrus - *Design of Axial Flow Fans with High Aerodynamic Loading*, Forschung im Ingenieurwesen-Engineering Research, Bd.62, Nr.3, S.58-64, **1996**.

[4] V.Cyrus, P. Wurst, J.Polansky - *Advanced Axial Flow Fan Stage for Power Stations with Environmental Equipment.* Proceedings of 7th European conference on Turbomachinery Fluid dynamics and Thermodynamics, pp. 34-45, Athens, **2007**

[5] V.Cyrus, P.Wurst – *High Pressure Axial Flow Fans for Power Industry*, Proceedings of 9th European conference on Turbomachinery Fluid dynamics and Thermodynamics, pp. 81-93, Istanbul, **2011**

[6] S. Lieblein - *Experimental Flow in Two-dimensional Cascades*. NASA SP 36, p.183, **1966**

[7] - Numeca Manuals, **2010**

[8] C. Clemen, U. Stark., J Fridrics., S. Baumgarten and G. Kosyna – *Effect of meanline shape, sweep and dihedral on stator performance of highly loaded single stage axial flow low- speed compressor.* Proceedings of 5th European conference on Turbomachinery Fluid dynamics and Thermodynamics, pp. 34-45, Lille, **2005**

[9] S. Reising, J.Font Brossa, H. P. Schiffer – *CFD Analysis of hub corner stall and secondary flow in compressor stage with non-axisymmetric end-walls.* Proceedings of 8th European conference on Turbomachinery Fluid dynamics and Thermodynamics, pp. 23-27, Graz, **2009**

[10] D. Japikse, N.S.C. Baines - *Diffuser Design Technology*, Concepts ETI Inc., **1998**

[11] R.A. Wallis - *Axial Flow Fans & Ducts* John. Wiley and Sons. New York-Brisbane, **1983**

[12] - *Industrial fans-performance testing using standardized airways*. ISO Standards 5801, **1997**

LIST OF SYMBOLS

A flow area
c chord
ζ loss coefficient
DF diffusion factor
$DF= 1-w_2/w_1+ ((w_{u1} - w_{u2})/2\sigma\, w_1)$
h blade height
M_k torque
p_T total pressure
Q volume flow rate
r radius
s blade pitch
entropy
u_t peripheral velocity at casing
w velocity
z coordinate normal to hub
α flow angle

η efficiency $\eta = Q\, \Delta p_T/ (M_k\, \omega)$
σ cascade solidity $\sigma = c/s$
φ flow coefficient $\varphi = Q/(Au_t)$
ψ pressure coefficient $\psi = 2\ \Delta p_T /(\rho\, u_t^2)$
ω angular velocity
ρ density

Indexes

F fan
D design, diffuser
h, t hub, tip
m meridional, mean
R rotor
S stator
ST stage (rotor + stator)
u peripheral
1,2 inlet , outlet

APPENDIX -

Effect of the inlet chamber and the diffuser losses on the axial flow fan aerodynamic performance

The aerodynamic performance relationship of the fan stage blading (R+S) and the complete axial fan system can be analysed using one-dimensional simplified flow model. The total pressure increment of the flow in axial fan $\Delta p_{T,\,F}$ can be expressed as the difference between the stage total pressure increment $\Delta p_{T,\,ST}$ and the total pressure losses in both inlet $\Delta p_{T,\,IC}$ and outlet $\Delta p_{T,D}$ fan sections

$$\Delta p_{T,\,F} = \Delta p_{T,\,ST} - (\Delta p_{T,\,IC} + \Delta p_{T,D}). \qquad (1)$$

Energy loss in the inlet suction chamber can be expressed as $\Delta p_{T,\,IC} = \zeta_{IC}\, q_1$ and similarly for the fan diffuser loss $\Delta p_{T,D} = \zeta_D\, q_3$. If we assume axial flow in Planes 1 and 3 (Fig.1), then the dynamic pressure: $q_1 = q_3 = 0.5\rho\, w_a^2$, $w_a = Q/A$. Using the definition of coefficients φ, ψ, the efficiency η and the equation (1) we obtain the following relations

$$\eta_F / \eta_{ST} = 1 - (\zeta_{IC} + \zeta_D)\, \varphi^2 / \psi_{ST}\,, \qquad (2)$$

$$\psi_F / \psi_{ST} = 1 - (\zeta_{IC} + \zeta_D)\, \varphi^2 / \psi_{ST}. \qquad (3)$$

Relationships valid for efficiency (2) are shown in Fig.11 for two fan construction studies with different energy losses of inlet and outlet fan parts: $\zeta_{IC} + \zeta_D$ = 0,14 and 0,25. Curves for stage blading with efficiency value of η_{ST} = 0,90 and three typical values of pressure coefficient ψ_{ST}: 0,40, 0,8 and 1,6 are drawn.

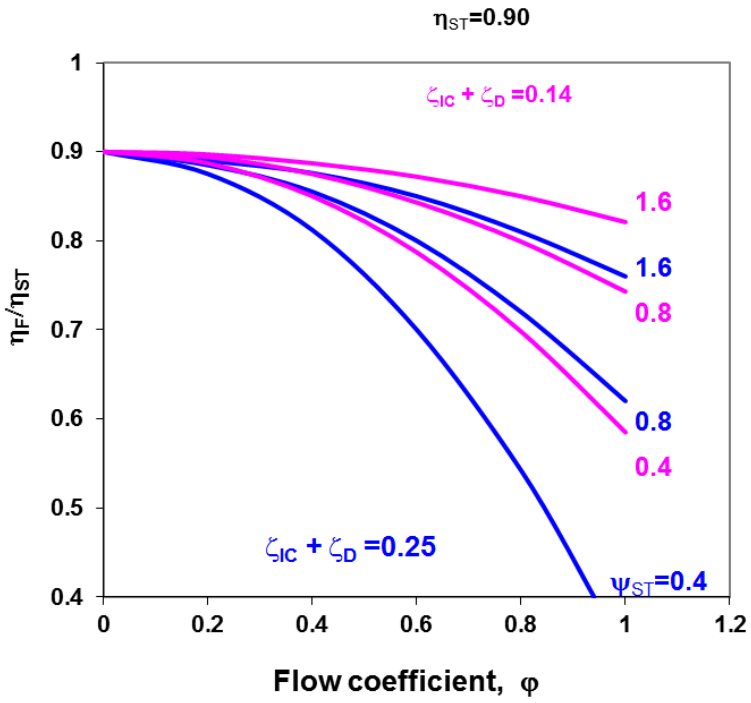

Figure 11: Fan efficiency dependence on flow coefficient